Dissolution Kinetics of a Three-Component Solid I: Ethylparaben, Phenacetin, and Salicylamide

MICHAEL SIMPSON and EUGENE L. PARROTT ˣ

Received March 12, 1982, from the *Division of Pharmaceutics, College of Pharmacy, University of Iowa, Iowa City, IA 52242.* Accepted for publication June 29, 1982.

Abstract □ The dissolution rates of each component in compressed spheres consisting of three components were measured under sink conditions. A film diffusion model is discussed and presented diagrammatically to illustrate the 13 possible dissolution behaviors of a three-component solid. Experimental dissolution rates compare favorably to dissolution rates calculated according to the model at mass fractions representative of the 13 dissolution behaviors

Keyphrases □ Ethylparaben—dissolution kinetics of a three-component solid, phenacetin, salicylamide □ Phenacetin—dissolution kinetics of a three-component solid, ethylparaben, salicylamide □ Salicylamide—dissolution kinetics of a three-component solid, ethylparaben, phenacetin

A limited number of reports on dissolution rates have been concerned with multicomponent solids. Recently, a general model for the dissolution rates of a nondisintegrating sphere composed of any number of components was presented (1). The purpose of this study was to develop a dissolution model for a three-component solid (ethylparaben, phenacetin, and salicylamide). The model suggests 13 possible dissolution behaviors, which are dependent on composition. A further purpose was to compare the experimental dissolution rates of each of the components with the dissolution rates predicted by the model.

EXPERIMENTAL

Preparation of Spheres—Twenty grams of each composition were prepared by blending the appropriate amounts of 60/80-mesh size fraction of ethylparaben[1], phenacetin[2], and salicylamide[3] for 15 min in a V-blender[4]. By means of a hydraulic press[5] fitted with a spherical punch and die set, each composition was compressed at a force of 2268 kg into spheres having a diameter of 1.273 ± 0.005 cm. The compositions (represented by solid circles) were selected according to the scheme shown in Fig. 1. Each corner of the triangle represents a compressed sphere composed of a single component. The three straight lines joining the corners of the triangle represent two-component compositions. Thus, the lines AB, BC, and AC represent two-component mixtures of A and B, B and C, and A and C, respectively. Each side of the triangle was divided into 10 equal segments. For example, a point on line AC midway between A and C represents a composition of 50% A and 50% C with no component B. The area within the triangle represents all mass fraction compositions of A, B, and C in a three-component system. The intercept of any three lines parallel to one of the lines AB, BC, and AC represents the composition of a particular three-component mixture. With high percentages of phenacetin the spheres were not readily formed, and heat was used to facilitate formation. With compositions containing ethylparaben the die was at 110°, and the force of compression was exerted for 3 min. In the absence of ethylparaben a temperature of 134° was used. Comparison of the dissolution rates of compacts made at room temperature to those made with heat showed that the difference did not exceed 2.7%, which was considered to be within experimental error.

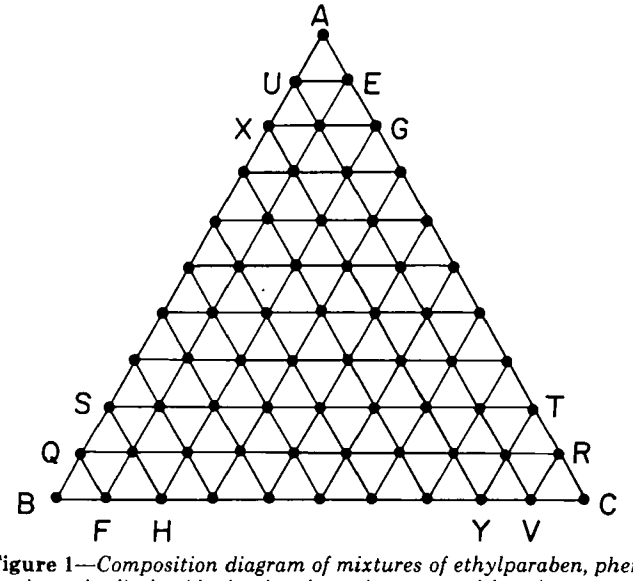

Figure 1—*Composition diagram of mixtures of ethylparaben, phenacetin, and salicylamide showing the various compositions (represented by solid circles) selected for investigation.*

Dissolution Rate—The dissolution rate was determined in distilled water at 25 ± 0.1°, as described previously (2, 3), under conditions where the concentration of the solutes did not exceed 5% of solubility. The dissolution apparatus and method were described previously (3, 4).

Solubility—Solubility measurements were made at 25°, as reported earlier (5). The solubilities of ethylparaben, phenacetin, and salicylamide are 0.939 ± 0.010, 0.842 ± 0.016, and 2.511 ± 0.018 mg/ml, respectively.

Analytical Procedure—The UV spectrum for each component was determined in a solution of that component containing 1.0 ml of 1.0 *N* sodium hydroxide in 25.0 ml of solution. The wavelengths of 296, 244, and 329 nm were selected. The standard curve of each component at each wavelength exhibited a Beer's law relationship. From these plots the nine

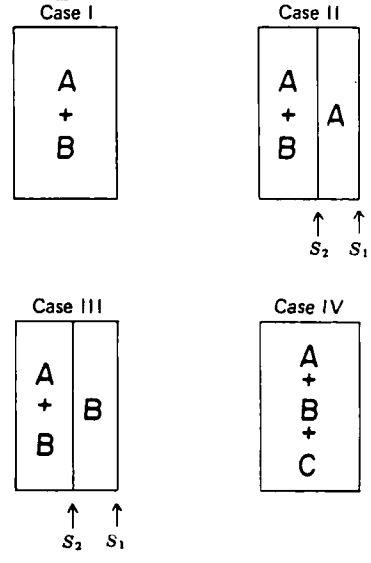

Figure 2—*Dissolution behaviors of two-component solids of components A and B and dissolution behavior of a three-component solid at its critical composition.*

[1] Sigma Chemical Co., Lot 117C-0156.
[2] Eastman, Lot A44.
[3] Sigma Chemical Co., Lot 107C-0409.
[4] Patterson-Kelly.
[5] Carver press, model C.

0022-3549/83/0700-0757$01.00/0

Table I—Molar Absorptivities of Ethylparaben, Phenacetin, and Salicylamide

Wavelength, nm	Molar Absorptivity		
	Ethylparaben	Phenacetin	Salicylamide
244	1,227	11,328	6,733
296	23,268	492	1,419
329	510	0	5,632

molar absorptivities were calculated (Table I). For a three-compartment system since absorbancies are additive:

$$A_1 = a_{11}C_A + a_{12}C_B + a_{13}C_C \quad \text{(Eq. 1)}$$

$$A_2 = a_{21}C_A + a_{22}C_B + a_{23}C_C \quad \text{(Eq. 2)}$$

$$A_3 = a_{31}C_A + a_{32}C_B + a_{33}C_C \quad \text{(Eq. 3)}$$

in which a_{ij} is the molar absorptivity of the species i at wavelength j, and A_j is the absorbance of the mixture at wavelength j. When the values of A_j and a_{ij} are substituted into Eqs. 1–3, and the equations are solved simultaneously, the concentrations C_A, C_B, and C_C are determined. Thus, the concentration of each component was obtained by UV absorbance at three selected wavelengths. The method was tested with seven solutions containing known concentrations of the three components. The percent determined by the analytical procedure ranged from 98.9 to 102.8% of the known concentration. The concentration was converted to amount dissolved in order to express a dissolution rate.

THEORY

With the dissolution of three-component solids if one assumes a Noyes–Whitney film theory, there are 13 dissolution behaviors possible. In Case IV dissolution behavior as shown in Fig. 2, the three components coexist at the solid–liquid interface, because as dissolution proceeds their boundaries recede at the same rate. This dissolution behavior occurs at a unique composition (critical composition) of the components at which:

$$\frac{N_A}{N_B} = \frac{D_A C_A}{D_B C_B} \quad \text{(Eq. 4)}$$

$$\frac{N_A}{N_C} = \frac{D_A C_A}{D_C C_C} \quad \text{(Eq. 5)}$$

and

$$\frac{N_B}{N_C} = \frac{D_B C_B}{D_C C_C} \quad \text{(Eq. 6)}$$

where N_A, N_B, and N_C are the mass fractions of components designated in general as A, B, and C; C_A, C_B, and C_C are their solubilities; and D_A, D_B, and D_C are their diffusion coefficients, respectively.

In Case V component C dissolves faster than components A and B, and

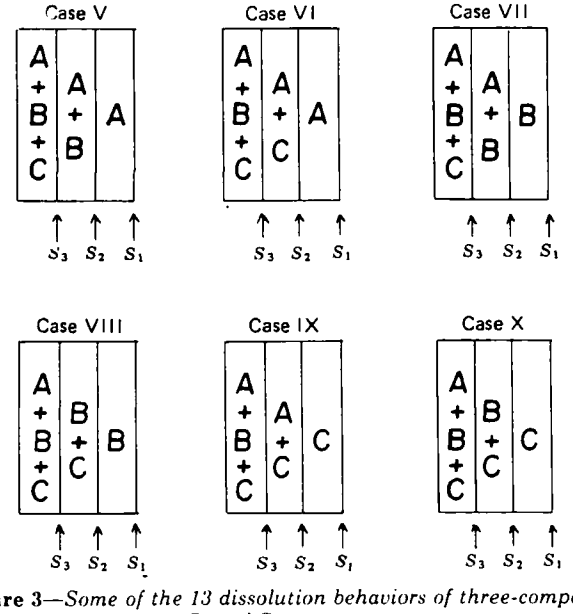

Figure 3—*Some of the 13 dissolution behaviors of three-component solids of components A, B, and C.*

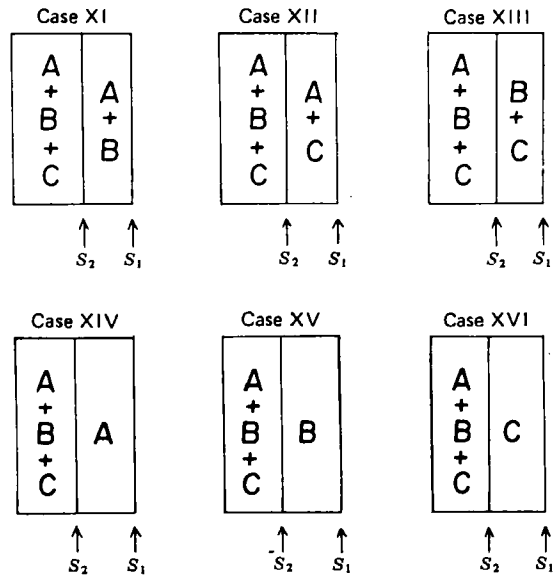

Figure 4—*Other possible dissolution behaviors of three-component solids of components A, B, and C.*

the dissolving boundary of component C recedes into the solid, as shown in Fig. 3. Component B dissolves faster from the solid surface than component A, so that the dissolving boundary of component B recedes within the solid leaving a surface layer of component A. Case V dissolution behavior occurs under the condition that:

$$\frac{N_A}{N_B} > \frac{D_A C_A}{D_B C_B} \quad \text{(Eq. 7)}$$

$$\frac{N_A}{N_C} > \frac{D_A C_A}{D_C C_C} \quad \text{(Eq. 8)}$$

and

$$\frac{N_B}{N_C} > \frac{D_B C_B}{D_C C_C} \quad \text{(Eq. 9)}$$

Cases VI, VII, VIII, IX, and X in Fig. 3 describe dissolution behaviors similar to Case V; however, the order of dissolving and the receding of the boundaries are different with different mass fractions of components A, B, and C.

In Case XI component C dissolves faster than the other two components and as dissolution proceeds the boundary of component C recedes within the solid leaving a layer of components A and B, which coexists

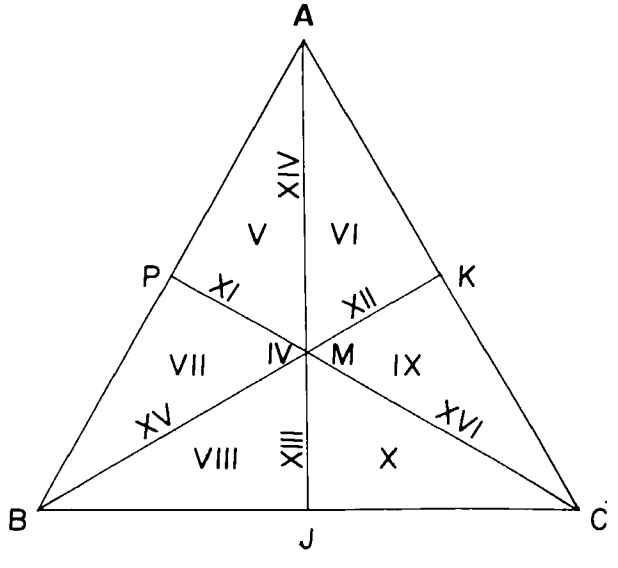

Figure 5—*Composition diagram for a three-component mixture of components having equal solubilities and diffusion coefficients showing the regions corresponding to the 13 dissolution behaviors. Roman numerals refer to the use of dissolution behavior described in the text.*

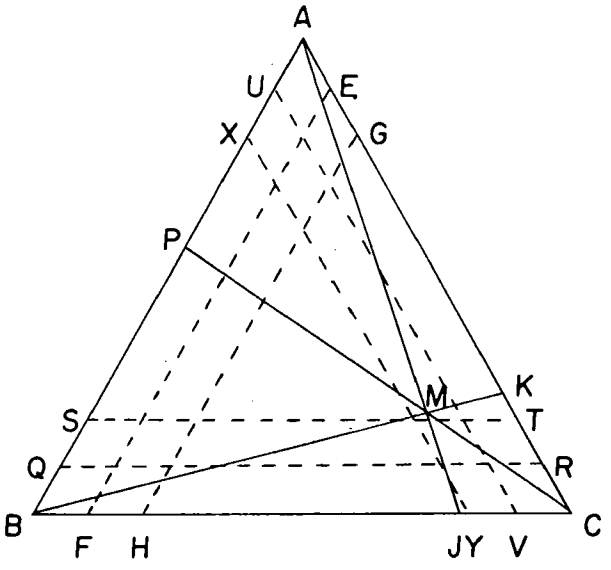

Figure 6—*Composition diagram for mixtures of ethylparaben, phenacetin, and salicylamide showing the regions corresponding to the 13 dissolution behaviors and their relationship to the compositions selected for investigation according to Fig. 1.*

at the surface, as shown in Fig. 4. Case XI dissolution behavior occurs under the conditions that:

$$\frac{N_A}{N_C} > \frac{D_A C_A}{D_C C_C} \quad \text{(Eq. 10)}$$

$$\frac{N_B}{N_C} > \frac{D_B C_B}{D_C C_C} \quad \text{(Eq. 11)}$$

and

$$\frac{N_A}{N_B} = \frac{D_A C_A}{D_B C_B} \quad \text{(Eq. 12)}$$

Cases XII and XIII in Fig. 4 describe dissolution behaviors similar to Case XI; however, the order of dissolving and the receding of the boundaries are different with different mass fractions of components A, B, and C.

In Case XIV both components B and C dissolve faster than component A and at the same rate, so that the boundaries of components B and C recede at the same rate and both coexist at the same boundary leaving a surface layer of component A. Case XIV dissolution behavior occurs under the conditions that:

$$\frac{N_A}{N_B} > \frac{D_A C_A}{D_B C_B} \quad \text{(Eq. 13)}$$

$$\frac{N_A}{N_C} > \frac{D_A C_A}{D_C C_C} \quad \text{(Eq. 14)}$$

and

$$\frac{N_B}{N_C} = \frac{D_B C_B}{D_C C_C} \quad \text{(Eq. 15)}$$

Cases XV and XVI in Fig. 4 describe dissolution behaviors similar to Case XIV; however, the order of dissolving and the receding of the boundaries are different with different mass fractions of components A, B, and C.

Using any two combinations of Eqs. 4, 5, or 6 and Eq. 16,

$$N_A + N_B + N_C = 1 \quad \text{(Eq. 16)}$$

the critical composition of components A, B, and C may be calculated. Similarly, for two-component mixtures of components A and B, components A and C, and components B and C, the critical composition may be calculated by use of the appropriate relationships. Dissolution behaviors of two-component solids have been previously described (6) and are presented as Cases I, II, and III in Fig. 2. Using these critical compositions a composition diagram can be drawn for a three-component system. Figure 5 shows the compositions corresponding to the 13 dissolution behaviors cited for three hypothetical components, which have equal solubilities and diffusion coefficients. Case IV dissolution behavior

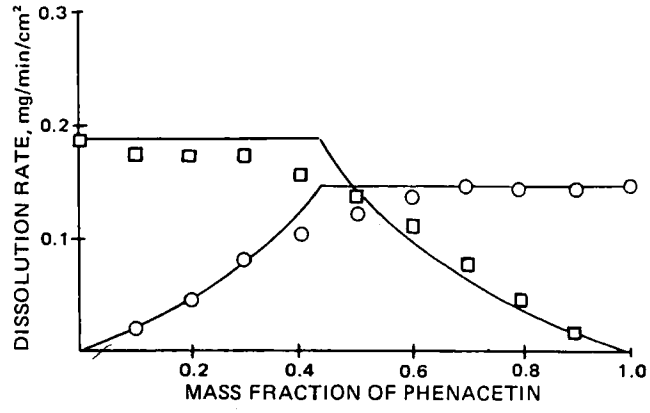

Figure 7—*Comparison of experimental dissolution rates of the components of ethylparaben and phenacetin mixtures corresponding to line AB of Fig. 1 and the smooth curves representing the theoretical rates. Key: (□) ethylparaben; (○) phenacetin.*

at the critical composition of the three-component mixture is represented by point M. Points P, J, and K represent the critical compositions of two-component mixtures of components A and B, components B and C, and components A and C, respectively. The line AMJ represents a three-component mixture, which contains components B and C (both in a mass fraction the same as the critical mass fraction for a two-component mixture of components B and C) with component A. From A to J the mass fraction of component A decreases while the mass fractions of components B and C increase.

The region APMK represents the condition in which components B and C have their boundaries within the solid coexisting, or following one another, depending on which portion is being considered. If the compositions of the three-component mixtures are on the line AM, there is a Case XIV dissolution behavior in which both components B and C coexist and have dissolving and receding boundaries within the solid, and component A is at the surface of the solid. Compositions within the region APM represent Case V dissolution behavior in which the dissolving boundary is deeper for component C than for component B, which in turn is deeper than that of component A, the surface component. Compositions within the region AMK represent Case VI dissolution behavior in which the dissolving boundary is deeper for component B than for component C, which in turn is deeper than that of component A, the surface component. Similarly, Case XI is represented by line PM; Case XII is represented by line MK; Case XIII is represented by line MJ; Case XIV is represented by line AM; Case XV is represented by line BM; and Case XVI is represented by line CM. Case VII is represented by the region BMP; Case VIII is represented by the region BMJ; Case X is represented by the region CMJ; and Case IX is represented by the region CMK.

The derivation of equations to describe dissolution of a three-component solid is illustrated for Case V dissolution behavior. Let S_1, S_2, and S_3 be the coordinate values representing the component A–solution boundary, component A–components A and B boundary, and compo-

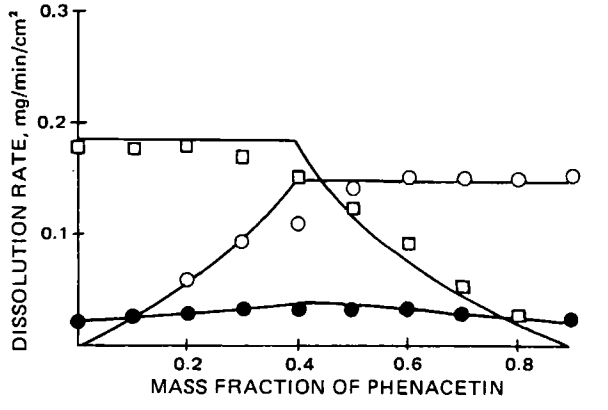

Figure 8—*Comparison of experimental dissolution rates of the components of ethylparaben, phenacetin, and salicylamide mixtures with a constant mass fraction of 0.1 salicylamide corresponding to line EF of Fig. 1 and the curves representing the theoretical rates. Key: (□) ethylparaben; (○) phenacetin; (●) salicylamide.*

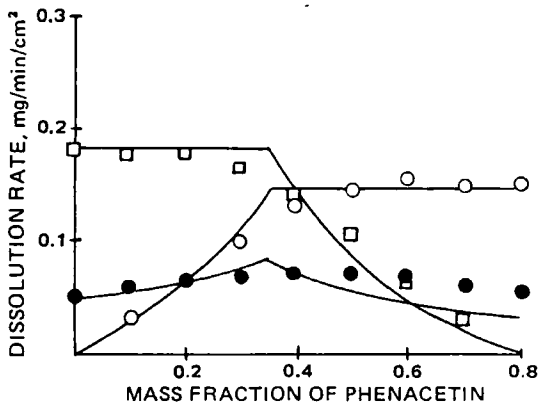

Figure 9—*Comparison of experimental dissolution rates of the components of ethylparaben, phenacetin, and salicylamide mixtures with a constant mass fraction of 0.2 salicylamide corresponding to line GH of Fig. 1 and the curves representing the theoretical rates. Key: (□) ethylparaben; (○) phenacetin; (●) salicylamide.*

nents A, B, and C–components A and B boundary, respectively. These are defined so that at a time $t = 0, S_3 = S_2 = S_1 = 0$. At $t > 0, S_2 - S_1$ is the thickness of the layer of component A, and $S_3 - S_2$ is the thickness of the layer of components A and B. Since component A is always on the surface, the dissolution rate (R_A) of component A is:

$$R_A = \frac{D_A C_A}{h} \qquad \text{(Eq. 17)}$$

where h is the effective diffusion layer thickness.

Component B must diffuse through the layer of component A of thickness $S_2 - S_1$, porosity ϵ_1, and tortuosity τ_1, and the liquid diffusion layer. The dissolution rate (R_B) of component B is:

$$R_B = \frac{D_B C_B}{h + (\tau_1/\epsilon_1)(S_2 - S_1)} \qquad \text{(Eq. 18)}$$

Component C must diffuse not only through the liquid diffusion layer but also through the interstitial space between the undissolved components A and B of thickness, $S_3 - S_2$, porosity, ϵ_2, and tortuosity, τ_2, and through the layer of component A of thickness $S_2 - S_1$, porosity ϵ_1, and tortuosity τ_1. The dissolution rate (R_C) of component C is:

$$R_C = \frac{D_C C_C}{h + (\tau_1/\epsilon_1)(S_2 - S_1) + (\tau_2/\epsilon_2)(S_3 - S_2)} \qquad \text{(Eq. 19)}$$

The dissolution rates may also be expressed:

$$R_A = A_A \frac{dS_1}{dt} \qquad \text{(Eq. 20)}$$

$$R_B = A_B \frac{dS_2}{dt} \qquad \text{(Eq. 21)}$$

$$R_C = A_C \frac{dS_3}{dt} \qquad \text{(Eq. 22)}$$

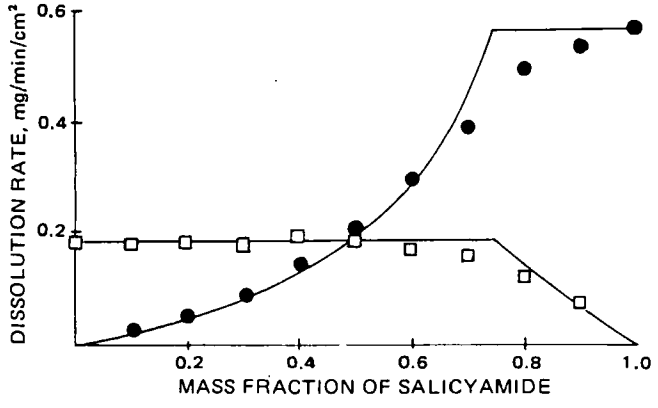

Figure 10—*Comparison of experimental dissolution rates of the components of ethylparaben and salicylamide mixtures corresponding to line AC of Fig. 1 and the smooth curves representing the theoretical dissolution rates. Key: (□) ethylparaben; (●) salicylamide.*

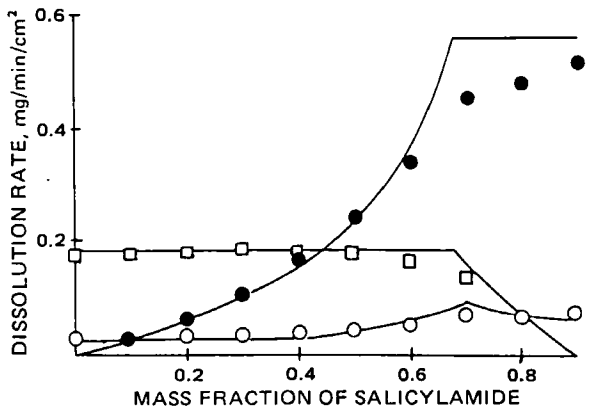

Figure 11—*Comparison of experimental dissolution rates of the components of ethylparaben, phenacetin, and salicylamide mixtures with a constant mass fraction of 0.1 phenacetin corresponding to line UV of Fig. 1 and the curves representing the theoretical rates. Key: (□) ethylparaben; (○) phenacetin; (●) salicylamide.*

where A_A, A_B, and A_C are the amounts per unit volume of component A, B, and C in the mixture. These equations state that the dissolution rate of a component is the product of the rate of movement of its boundary and the concentration in that layer. The amount of components B and C remaining in solution in the pores have not been considered. As the dissolution rate of component A is represented by Eqs. 17 and 20, it follows that:

$$A_A \frac{dS_1}{dt} = \frac{D_A C_A}{h} \qquad \text{(Eq. 23)}$$

$$\frac{dS_1}{dt} = \frac{D_A C_A}{A_A h} \qquad \text{(Eq. 24)}$$

When $S_1 = 0$ at $t = 0$, the solution to Eq. 24 is:

$$S_1 = \frac{D_A C_A t}{A_A h} \qquad \text{(Eq. 25)}$$

Substituting Eq. 25 into Eq. 18 and combining it with Eq. 22 yields:

$$\frac{dS_2}{dt} = \frac{D_B C_B}{A_B[h + (\tau_1/\epsilon_1)(S_2 - D_A C_A t/h)]} \qquad \text{(Eq. 26)}$$

$$= \frac{K_2}{h + (\tau_1/\epsilon_1)(S_2 - K_1 t)} \qquad \text{(Eq. 27)}$$

where $K_1 = D_A C_A / A_A h$ and $K_2 = D_B C_B / A_B$.

Using Laplace transforms (7) if $S_2 = 0$ at $t = 0$, the solution to Eq. 27 is:

$$t = 1/K_1[S_2 - (\epsilon_1/\tau_1)(K_2/K_1 - h)(1 - \exp -(K_1\tau_1/K_2\epsilon_1)S_2)] \qquad \text{(Eq. 28)}$$

If $S_2 \gg \epsilon_1 K_2/\tau_1 K_1 = \epsilon_1 D_B C_B A_A h/\tau_1 D_A C_A A_B$, Eq. 28 is approximately:

$$t = 1/K_1[S_2 - (\epsilon_1/\tau_1)(K_2/K_1 - h)] \qquad \text{(Eq. 29)}$$

which may be rearranged to:

$$S_2 = K_1 t + (\epsilon_1/\tau_1)(K_2/K_1 - h) \qquad \text{(Eq. 30)}$$

Differentiation of Eq. 30 yields:

$$\frac{dS_2}{dt} = K_1 = \frac{D_A C_A}{A_A h} \qquad \text{(Eq. 31)}$$

Substitution of Eq. 31 into Eq. 21 yields:

$$R_B = \frac{A_B D_A C_A}{A_A h} \qquad \text{(Eq. 32)}$$

$$R_B = \frac{N_B}{N_A} R_A \qquad \text{(Eq. 33)}$$

where N_A and N_B are the mass fractions of component A and B, respectively.

To derive the equation for the dissolution rate of component C, Eqs. 25 and 30 are substituted into Eq. 19 to yield:

$$R_C = \frac{D_C C_C}{h + (\tau_1/\epsilon_1)(K_1 t + Y - K_1 t) + (\tau_2/\epsilon_2)[S_3 - (K_1 t + Y)]} \qquad \text{(Eq. 34)}$$

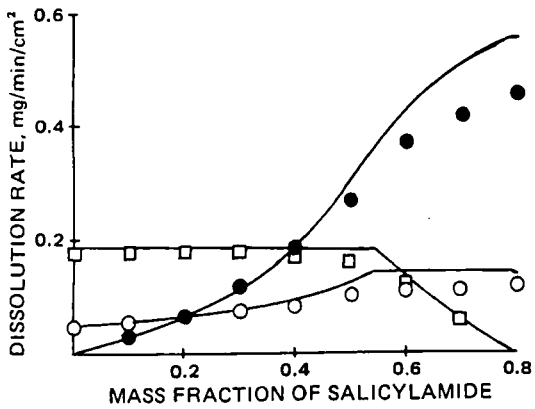

Figure 12—*Comparison of experimental dissolution rates of the components of ethylparaben, phenacetin, and salicylamide mixtures with a constant mass fraction of 0.2 phenacetin corresponding to line XY of Fig. 1 and the curves representing the theoretical rates. Key: (□) ethylparaben; (○) phenacetin; (●) salicylamide.*

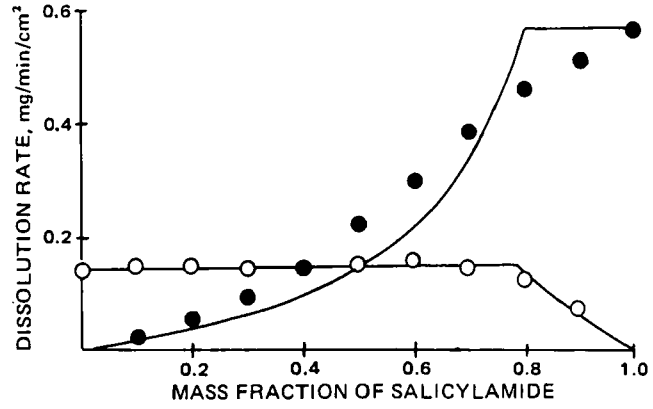

Figure 13—*Comparison of experimental dissolution rates of the components of phenacetin and salicylamide mixtures corresponding to line BC of Fig. 1 and the curves representing the theoretical rates. Key: (○) phenacetin; (●) salicylamide.*

where $Y = (\epsilon_1/\tau_1)(K_2/K_1 - h)$. Combining of Eqs. 22 and 34:

$$\frac{dS_3}{dt} = \frac{K_3}{h + (\tau_1/\epsilon_1)(Y) + (\tau_2/\epsilon_2)[S_3 - (K_1t + Y)]} \quad \text{(Eq. 35)}$$

and $K_3 = D_C C_C / A_C$.

Using Laplace transforms, the solution to Eq. 35 is:

$$t = 1/K_1[S_3 + (\epsilon_2/\tau_2)(K_3K_4 - K_3/K_1) \times (1 - \exp -(\tau_2K_1/\epsilon_2K_3)S_3)] \quad \text{(Eq. 36)}$$

where $K_4 = 1/K_3[h + Y([\tau_1/\epsilon_1] - [\tau_2/\epsilon_2])]$ and $Y = (\epsilon_1/\tau_1)(K_2/K_1 - h)$. If $S_3 \gg \epsilon_2K_3/\iota_2K_1 = \epsilon_2D_CC_CA_Ah/\tau_2D_AC_AA_C$, Eq. 36 simplifies to:

$$t = 1/K_1[S_3 + (\epsilon_2/\tau_2)(K_3K_4 - K_3/K_1)] \quad \text{(Eq. 37)}$$

Differentiating Eq. 37:

$$\frac{dS_3}{dt} = K_1 \quad \text{(Eq. 38)}$$

where $K_1 = D_AC_A/A_Ah$. Substituting Eq. 37 into Eq. 22:

$$R_C = \frac{A_CD_AC_A}{A_Ah} \quad \text{(Eq. 39)}$$

$$R_C = \frac{N_C}{N_A}R_A \quad \text{(Eq. 40)}$$

Equations 17, 33, and 40 may be used to calculate the theoretical dissolution rates of each of the components in a three-component mixture with the dissolution behaviors represented by Cases VI, VII, VIII, IX, and X.

By differential equations similar to those employed in the discussion of Case V dissolution behavior, the theoretical dissolution rate equations for Case XI dissolution behavior are:

$$R_A = \frac{D_AC_A}{h} \quad \text{(Eq. 41)}$$

$$R_B = \frac{D_BC_B}{h} \quad \text{(Eq. 42)}$$

$$R_C = \frac{N_C}{N_A}R_A = \frac{N_C}{N_B}R_B \quad \text{(Eq. 43)}$$

The dissolution rate equations for Case XII and XIII dissolution behavior are similar to those of Case XI.

The dissolution rate equations for Case XIV dissolution behavior are:

$$R_A = \frac{D_AC_A}{h} \quad \text{(Eq. 44)}$$

$$R_B = \frac{N_B}{N_A}R_A \quad \text{(Eq. 45)}$$

$$R_C = \frac{N_C}{N_A}R_A \quad \text{(Eq. 46)}$$

The dissolution rate equations for Case XV and XVI dissolution behavior are similar to those of Case XIV.

The dissolution rate equations for Case IV dissolution behavior are

$$R_A = \frac{D_AC_A}{h} \quad \text{(Eq. 47)}$$

$$R_B = \frac{D_CC_B}{h} \quad \text{(Eq. 48)}$$

$$R_C = \frac{D_CC_C}{h} \quad \text{(Eq. 49)}$$

as the three components coexist at the solid–liquid interface.

RESULTS AND DISCUSSION

Dissolution rates were measured at 25° under sink conditions at the various compositions shown as solid circles in Fig. 1 on lines AB, EF, GH, AC, UV, XY, BC, QR, and ST. For the system investigated A represents ethylparaben, B represents phenacetin, and C represents salicylamide. Lines AB, EF, and GH correspond to varying compositions of ethylparaben and phenacetin with a constant mass fraction of salicylamide of 0, 0.1, and 0.2, respectively. A similar interpretation is given to the other axes of the ternary diagram.

Dissolution rates were measured under identical experimental conditions used previously (3) to determine the effective diffusion layer thickness to be 3×10^{-3} cm. The solubility was experimentally measured. When the dissolution of a nondisintegrating pure solid occurring in a nonreactive medium at sink conditions is diffusion controlled, the dissolution rate may be expressed as (5):

$$R = \frac{DC_s}{h} \quad \text{(Eq. 50)}$$

The only unknown term in Eq. 50 is the diffusion coefficient. Rearranging Eq. 50 and substituting the experimental values for ethylparaben gives:

$$D = \frac{0.0031 \times 3 \times 10^{-3}}{0.939} = 1.00 \times 10^{-5} \text{ cm}^2/\text{sec} \quad \text{(Eq. 51)}$$

In a similar manner the diffusion coefficients of phenacetin and salicylamide were found to be 0.86×10^{-5} and 1.124×10^{-5} cm²/sec, respectively.

To determine the critical composition at which each of the components coexist at the solid–liquid interface with their dissolving boundaries receding at the same rate, the values of the diffusion coefficient and the solubility of the components were substituted into any two combinations of Eqs. 4, 5, or 6 with Eq. 16. By simultaneous solution the critical mass fractions are 0.209 ethylparaben, 0.163 phenacetin, and 0.628 salicylamide.

Similarly, by using the values of solubility and diffusion coefficient and appropriate equations (6), the critical mass fractions for two-component mixtures were calculated. The critical mass fractions are 0.562 ethylparaben and 0.438 phenacetin, 0.25 ethylparaben and 0.75 salicylamide, and 0.794 phenacetin and 0.206 salicylamide.

With these critical compositions for two- and three-component mixtures, Fig. 6 was constructed to show the regions that represent 13 dissolution behaviors and the lines of Fig. 1 from which the various com-

positions were chosen for investigation. By consideration of Fig. 6 and by then employing appropriate equations, the theoretical dissolution rates were calculated from dissolution behavior in the various regions of the diagram.

For Case IV dissolution behavior at the critical composition of the three components, the boundaries recede at the same rate, and the dissolution rates according to Eqs. 47–49 are:

$$R_A = \frac{1.00 \times 10^{-5} \times 0.939}{3 \times 10^{-3}} = 0.0031 \text{ mg/sec/cm}^2 \ (0.188 \text{ mg/min/cm}^2) \quad \text{(Eq. 52)}$$

$$R_B = \frac{0.86 \times 10^{-5} \times 0.842}{3 \times 10^{-3}} = 0.0024 \text{ mg/sec/cm}^2 \ (0.145 \text{ mg/min/cm}^2) \quad \text{(Eq. 53)}$$

$$R_C = \frac{1.124 \times 10^{-5} \times 2.511}{3 \times 10^{-3}} = 0.0094 \text{ mg/sec/cm}^2 \ (0.565 \text{ mg/min/cm}^2) \quad \text{(Eq. 54)}$$

To illustrate other calculations, consider the line QR passing through the regions BMP, BJM, CMJ, and CKM of Fig. 6. In the BMP region the dissolution behavior described as Case VII exists. A composition of 0.75 phenacetin, 0.10 ethylparaben, and 0.15 salicylamide on line QR lies in this regions in which:

$$\frac{N_B}{N_A} > \frac{D_B C_B}{D_A C_A} \quad \text{(Eq. 55)}$$

and

$$\frac{N_B}{N_C} > \frac{D_B C_B}{D_C C_C} \quad \text{(Eq. 56)}$$

Thus, phenacetin exists in a layer at the solid surface while the boundaries of ethylparaben and salicylamide have receded into the solid. At this composition:

$$\frac{N_A}{N_C} > \frac{D_A C_A}{D_C C_C} \quad \text{(Eq. 57)}$$

so that the dissolving and receding boundary of salicylamide recedes further than that of ethylparaben.

The dissolution rate of phenacetin according to Eq. 50 is:

$$R_B = \frac{0.86 \times 10^{-5} \times 0.842}{3 \times 10^{-3}} = 0.0024 \text{ mg/sec/cm}^2 \ (0.145 \text{ mg/min/cm}^2) \quad \text{(Eq. 58)}$$

The dissolution rates of ethylparaben and salicylamide are:

$$R_A = \frac{0.1}{0.75} \times 0.145 = 0.019 \text{ mg/min/cm}^2 \quad \text{(Eq. 59)}$$

and

$$R_C = \frac{0.15}{0.75} \times 0.145 = 0.029 \text{ mg/min/cm}^2 \quad \text{(Eq. 60)}$$

according to Eqs. 33 and 40.

For a solid composition of three components with mass fractions of 0.1 ethylparaben, 0.6 phenacetin, and 0.3 salicylamide on lines QR and BM separating regions BMP and BJM of Fig. 6:

$$\frac{N_B}{N_A} > \frac{D_B C_B}{D_A C_A} \quad \text{(Eq. 61)}$$

$$\frac{N_B}{N_C} > \frac{D_B C_B}{D_C C_C} \quad \text{(Eq. 62)}$$

and

$$\frac{N_A}{N_C} = \frac{D_C C_A}{D_C C_C} \quad \text{(Eq. 63)}$$

This composition is described as Case XV dissolution behavior in which both ethylparaben and salicylamide have their dissolving and receding boundaries at the same rate within the solid leaving phenacetin at the solid surface.

The dissolution rate of phenacetin according to Eq. 50 is 0.145 mg/min/cm^2. The dissolution rates of ethylparaben and salicylamide are:

$$R_A = \frac{0.1}{0.6} \times 0.145 = 0.023 \text{ mg/min/cm}^2 \quad \text{(Eq. 64)}$$

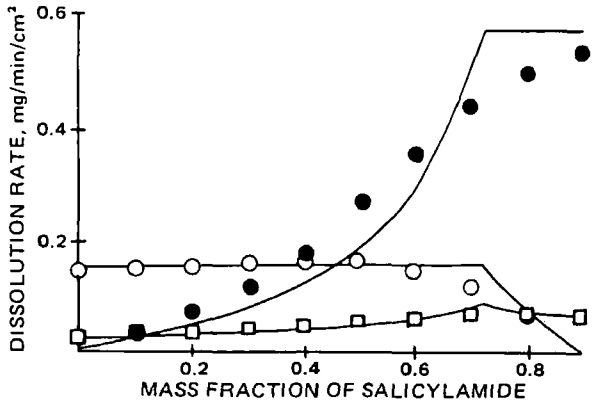

Figure 14—*Comparison of experimental dissolution rates of the components of ethylparaben, phenacetin, and salicylamide mixtures with a constant mass fraction of 0.1 ethylparaben corresponding to line QR of Fig. 1 and the curves representing the theoretical rates. Key: (□) ethylparaben; (○) phenacetin; (●) salicylamide.*

and

$$R_C = \frac{0.3}{0.6} \times 0.145 = 0.073 \text{ mg/min/cm}^2 \quad \text{(Eq. 65)}$$

according to Eqs. 45 and 46.

A solid composition of 0.1 ethylparaben, 0.4 phenacetin, and 0.5 salicylamide is described by Case VIII dissolution behavior in region BJM in which:

$$\frac{N_B}{N_A} > \frac{D_B C_B}{D_A C_A} \quad \text{(Eq. 66)}$$

$$\frac{N_B}{N_C} > \frac{D_B C_B}{D_C C_C} \quad \text{(Eq. 67)}$$

and

$$\frac{N_C}{N_A} > \frac{D_C C_C}{D_A C_A} \quad \text{(Eq. 68)}$$

The dissolution rate of phenacetin according to Eq. 50 is 0.145 mg/min/cm^2. The dissolution rates of salicylamide and ethylparaben are:

$$R_C = \frac{0.5}{0.4} \times 0.145 = 0.181 \text{ mg/min/cm}^2 \quad \text{(Eq. 69)}$$

and

$$R_A = \frac{0.1}{0.4} \times 0.145 = 0.036 \text{ mg/min/cm}^2 \quad \text{(Eq. 70)}$$

A solid composition of three components with mass fractions of 0.1 ethylparaben, 0.184 phenacetin, and 0.716 salicylamide on line QR is described by Case XIII dissolution behavior on line JM (which separates regions BJM and CMJ) on which:

$$\frac{N_A}{N_B} < \frac{D_A C_A}{D_B C_B} \quad \text{(Eq. 71)}$$

$$\frac{N_A}{N_C} < \frac{D_A C_A}{D_C C_C} \quad \text{(Eq. 72)}$$

and

$$\frac{N_B}{N_C} = \frac{D_B C_B}{D_C C_C} \quad \text{(Eq. 73)}$$

The dissolution rates of phenacetin and salicylamide according to Eqs. 41 and 42 are 0.145 and 0.565 mg/min/cm^2. The dissolution rate of ethylparaben according to Eq. 43 is:

$$R_A = \frac{0.1}{0.184} \times 0.145 = 0.079 \text{ mg/min/cm}^2 \quad \text{(Eq. 74)}$$

A solid with a mass fraction of 0.1 ethylparaben, 0.13 phenacetin, and

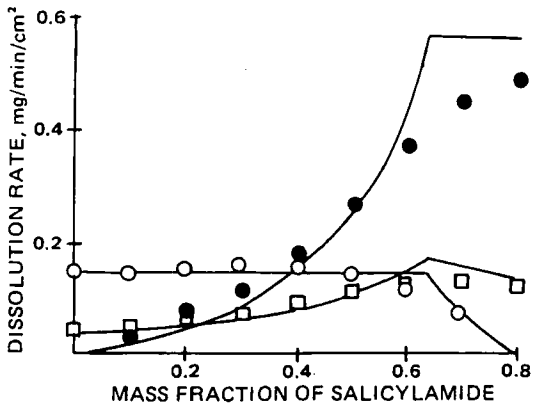

Figure 15—*Comparison of experimental dissolution rates of the components of ethylparaben, phenacetin, and salicylamide mixtures with a constant mass fraction of 0.2 ethylparaben corresponding to line ST of Fig. 1 and the curves representing the theoretical rates. Key: (□) ethylparaben; (○) phenacetin; (●) salicylamide.*

0.77 salicylamide on line QR has a Case X dissolution behavior in the region CMJ in which:

$$\frac{N_C}{N_A} > \frac{D_C C_C}{D_A C_A} \quad \text{(Eq. 75)}$$

$$\frac{N_C}{N_B} > \frac{D_C C_C}{D_B C_B} \quad \text{(Eq. 76)}$$

and

$$\frac{N_B}{N_A} > \frac{D_B C_B}{D_A C_A} \quad \text{(Eq. 77)}$$

In Case X dissolution behavior the dissolving and receding boundary of ethylparaben is deepest within the solid, the boundary of salicylamide is at the surface, and the boundary of phenacetin is between the two boundaries. The dissolution rate of salicylamide according to Eq. 50 is 0.565 mg/min/cm². The dissolution rate of phenacetin is:

$$R_B = \frac{0.13}{0.77} \times 0.565 = 0.095 \text{ mg/min/cm}^2 \quad \text{(Eq. 78)}$$

The dissolution rate of ethylparaben is:

$$R_A = \frac{0.1}{0.77} \times 0.565 = 0.073 \text{ mg/min/cm}^2 \quad \text{(Eq. 79)}$$

A solid composition with mass fractions of 0.1 ethylparaben, 0.075 phenacetin, and 0.825 salicylamide on line QR is described by Case XVI dissolution behavior on line CM (which separates regions CMJ and CKM) on which:

$$\frac{N_C}{N_A} > \frac{D_C C_C}{D_A C_A} \quad \text{(Eq. 80)}$$

$$\frac{N_C}{N_B} > \frac{D_C C_C}{D_B C_B} \quad \text{(Eq. 81)}$$

and

$$\frac{N_A}{N_B} = \frac{D_A C_A}{D_B C_B} \quad \text{(Eq. 82)}$$

At this composition salicylamide forms the surface layer, and the dissolving and receding boundaries of ethylparaben and phenacetin recede at the same rate within the solid. The dissolution rate of salicylamide according to Eq. 50 is 0.565 mg/min/cm². The dissolution rate of ethylparaben is:

$$R_A = \frac{0.1}{0.825} \times 0.565 = 0.068 \text{ mg/min/cm}^2 \quad \text{(Eq. 83)}$$

The dissolution rate of phenacetin is:

$$R_B = \frac{0.075}{0.825} \times 0.565 = 0.051 \text{ mg/min/cm}^2 \quad \text{(Eq. 84)}$$

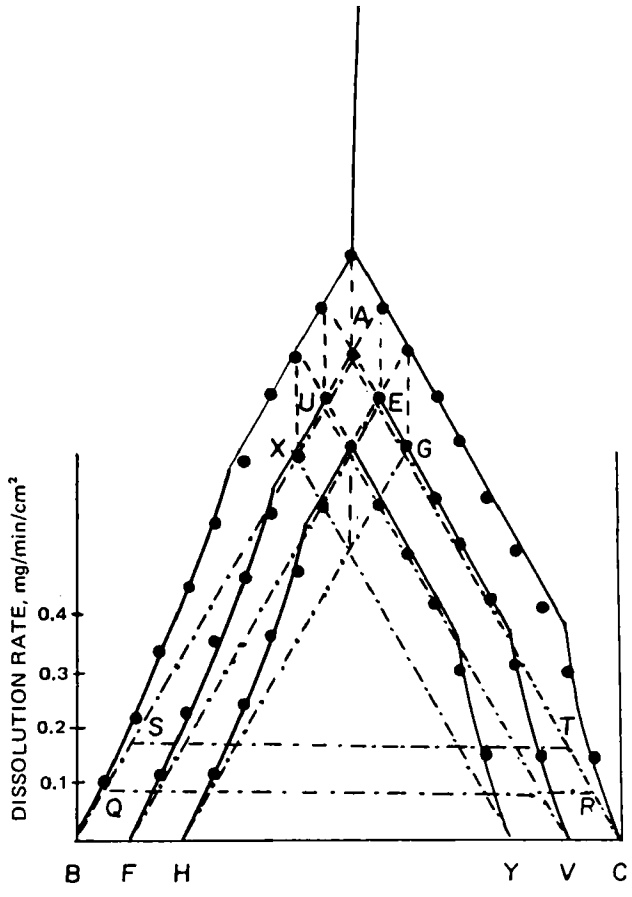

Figure 16—*Comparison of experimental dissolution rates of ethylparaben in solids of various compositions of ethylparaben, phenacetin, and salicylamide with theoretical dissolution rates represented by the solid lines in a three-dimensional perspective. Key: (A) ethylparaben; (B) phenacetin; (C) salicylamide.*

A solid composition with mass fractions of 0.1 ethylparaben, 0.05 phenacetin, and 0.85 salicylamide is described by Case IX dissolution behavior in region CKM in which the dissolving and receding boundary of phenacetin is deepest within the solid, the boundary of salicylamide is the surface layer, and the boundary of ethylparaben is between the two boundaries. The dissolution rate of salicylamide according to Eq. 50 is 0.565 mg/min/cm². The dissolution rate of ethylparaben is:

$$R_A = \frac{0.10}{0.85} \times 0.565 = 0.066 \text{ mg/min/cm}^2 \quad \text{(Eq. 85)}$$

The dissolution rate of phenacetin is:

$$R_B = \frac{0.05}{0.85} \times 0.565 = 0.033 \text{ mg/min/cm}^2 \quad \text{(Eq. 86)}$$

For two-component mixtures the dissolution rates were calculated according to the equations presented previously (6) for Cases I, II, and III. For example, a mixture of ethylparaben and phenacetin has a critical composition of 0.562 ethylparaben and 0.438 phenacetin at which:

$$\frac{N_A}{N_B} = \frac{D_A C_A}{D_B C_B} \quad \text{(Eq. 87)}$$

At the critical composition as represented by point P on line AB in Fig. 6, the dissolution rates of ethylparaben and phenacetin according to Eq. 50 are 0.188 and 0.145 mg/min/cm², respectively. A two-component solid composed of mass fractions of 0.3 ethylparaben and 0.7 phenacetin is represented by line BP on which:

$$\frac{N_A}{N_B} < \frac{D_A C_A}{D_B C_B} \quad \text{(Eq. 88)}$$

Phenacetin exists as the surface layer with the dissolving and receding boundary of ethylparaben within the solid. The dissolution rate of

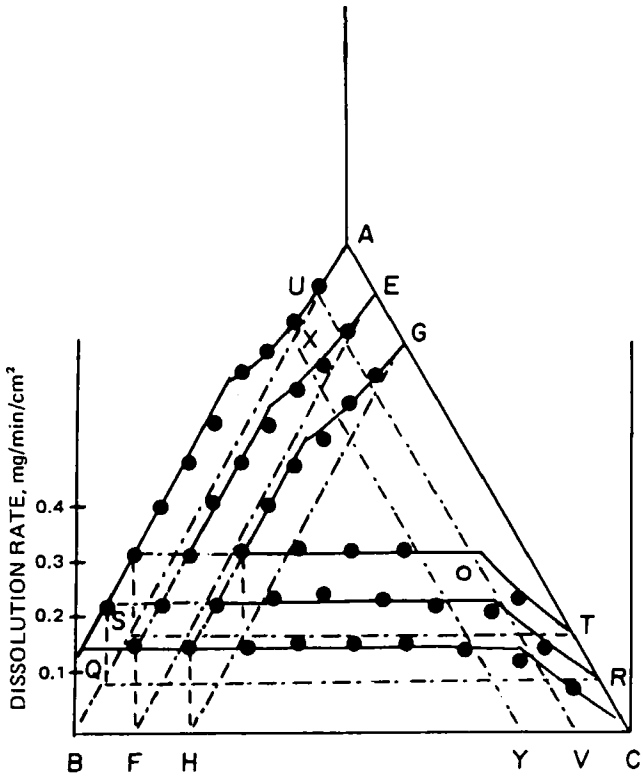

Figure 17—*Comparison of experimental dissolution rates of phenacetin in solids of various compositions of ethylparaben, phenacetin, and salicylamide with theoretical dissolution rates represented by solid lines in a three dimensional perspective. Key: (A) ethylparaben; (B) phenacetin; (C) salicylamide.*

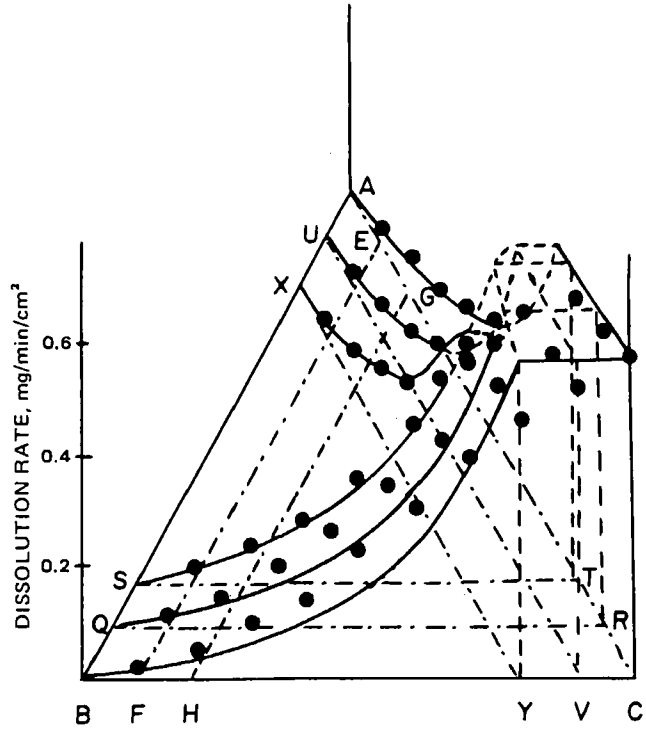

Figure 18—*Comparison of experimental dissolution rates of salicylamide in solids of various compositions of ethylparaben, phenacetin, and salicylamide with theoretical dissolution rates represented by the solid lines in a three dimensional perspective. Key: (A) ethylparaben; (B) phenacetin; (C) salicylamide.*

phenacetin according to Eq. 50 is 0.145 mg/min/cm^2. The dissolution rate of ethylparaben is:

$$R_A = \frac{0.3}{0.7} \times 0.145 = 0.062 \text{ mg/min/cm}^2 \quad \text{(Eq. 89)}$$

In a similar manner the predicted dissolution rates of each component were calculated and compared in Figs. 7–15 to the experimental dissolution rates at corresponding compositions. In Figs. 7, 10, and 13 the experimental dissolution rates of two-component mixtures of ethylparaben and phenacetin, ethylparaben and salicylamide, and phenacetin and salicyamide correspond in Fig. 6 to lines AB, AC, and BC, respectively. The experimental dissolution rates approximate the predicted dissolution rates for the ethylparaben and phenacetin mixture and for the ethylparaben and salicylamide mixture. As it has been observed previously (4, 6), the greatest difference between the predicted and experimental values occurs about the critical composition. This may result because the model ignores the amount of components in solution in the pores of the layers. In Fig. 13 for the phenacetin and salicylamide mixture, the experimental dissolution rates of salicylamide are faster than the predicted dissolution rates at mass fractions of 0.1–0.7 salicylamide. These faster dissolution rates may be attributed to the greater solubility of salicylamide, which dissolves faster leaving a surface layer of phenacetin. The mechanically weak surface of phenacetin, which possesses poor bonding characteristics, erodes slightly, and the increase in the effective surface area because of flaking results in a greater quantity dissolving per unit time.

In Figs. 8, 9, 11, 12, 14, and 15 the theoretical and experimental dissolution rates are compared for compositions in which the mass fraction of one component is constant and the mass fractions of the other components are varied. Figures 8 and 9 show the comparison of the predicted and experimental dissolution rates of ethylparaben, phenacetin, and salicylamide with a constant mass fraction of salicylamide of 0.1 and 0.2 corresponding to lines EF and GH, respectively, and varying mass fractions of ethylparaben and phenacetin. The predicted and experimental dissolution rates vary only about the critical composition. In Fig. 9 the experimental dissolution rates are faster than the predicted dissolution rates at mass fractions >0.5 phenacetin for solids with a constant mass fraction of 0.2 salicylamide. Again this may be attributed to the weak mechanical strength and consequential flaking due to the weak bonding of phenacetin.

The dissolution rates of ethylparaben, phenacetin, and salicylamide are shown in Figs. 11 and 12 with a constant mass fraction of phenacetin of 0.1 and 0.2 corresponding to lines UV and XY of Fig. 6. The dissolution rates of ethylparaben, phenacetin, and salicylamide are shown in Figs. 14 and 15 with a constant mass fraction of ethylparaben corresponding to lines QR and ST in Fig. 6.

A diagram of three-dimensional perspective is shown in Fig. 16 for the experimental and predicted dissolution rates of ethylparaben from three-component mixtures. Similarly, the experimental and predicted dissolution rates of phenacetin and salicylamide from three-component mixtures are presented in Figs. 17 and 18, respectively.

The experimental dissolution rates of the components of various compositions of ethylparaben, phenacetin, and salicylamide from compressed spheres essentially substantiates the suggested model for the dissolution kinetics of a three-component, nondisintegrating solid.

REFERENCES

(1) G. R. Carmichael, S. A. Shah, and E. L. Parrott, *J. Pharm. Sci.*, **70**, 1331 (1981).

(2) E. L. Parrott, D. E. Wurster, and T. Higuchi, *J. Am. Pharm. Assoc., Sci. Ed.*, **44**, 269 (1955).

(3) R. J. Braun and E. L. Parrott, *J. Pharm. Sci.*, **61**, 175 (1972).

(4) S. A. Shah and E. L. Parrott, *ibid.*, **65**, 1874 (1976).

(5) E. L. Parrott and V. K. Sharma, *ibid.*, **56**, 1341 (1967).

(6) W. I. Higuchi, N. A. Mir, and S. J. Desai, *ibid.*, **54**, 1405 (1965).

(7) E. D. Rainville, "The Laplace Transforms, An Introduction," Macmillan, New York, N.Y., 1963.

ACKNOWLEDGMENTS

Abstracted in part from a dissertation submitted by Michael Simpson to the Graduate College, University of Iowa in partial fulfillment of the Doctor of Philosophy degree requirements.